Journal of Nuclear Materials 444 (2014) 186–199

Contents lists available at ScienceDirect

Journal of Nuclear Materials

journal homepage: www.elsevier.com/locate/jnucmat

Thermal treatment of simulant plutonium contaminated materials from the Sellafield site by vitrification in a blast-furnace slag ☆

N.C. Hyatt [a,*], R.R. Schwarz [a], P.A. Bingham [a], M.C. Stennett [a], C.L. Corkhill [a], P.G. Heath [a], R.J. Hand [a], M. James [b], A. Pearson [b], S. Morgan [c]

[a] Department of Materials Science & Engineering, The University of Sheffield, Mappin Street, Sheffield S1 3JD, UK
[b] Sellafield Ltd., Sellafield, Seascale, Cumbria CA20 1PG, UK
[c] Sellafield Ltd., Hinton House, Risley, Warrington WA3 6GR, UK

GRAPHICAL ABSTRACT

Storage of 200 L drums of PCM waste at the Sellafield site, UK.

ARTICLE INFO

Article history:
Received 17 June 2013
Accepted 12 August 2013
Available online 22 August 2013

ABSTRACT

Four waste simulants, representative of Plutonium Contaminated Materials (PCMs) at the Sellafield site, were vitrified through additions of Ground Granulated Blast-furnace Slag (GGBS). Ce (as a Pu surrogate) was effectively partitioned into the slag product, enriched in an amorphous $CaO–Fe_2O_3–Al_2O_3–SiO_2$ phase when other crystalline phases were also present. Ce L_3 edge XANES data demonstrated Ce to be present as trivalent species in the slag fraction, irrespective of the waste type. Estimated volume reductions of ca. 80–95% were demonstrated, against a baseline of uncompacted 200 L PCM waste drums. The dissolution behaviour of PCM slag wasteforms was investigated at 50 °C in saturated $Ca(OH)_2$ solution under N_2 atmosphere, to simulate the hyperalkaline anoxic environment of a cementitious UK Geological Disposal Facility for Intermediate Level Waste (ILW). These experiments demonstrated the performance of the slag wasteforms to be comparable to that of other vitrified ILW materials considered potentially suitable for geological disposal.

* Corresponding author. Tel.: +44 (0)114 222 5470; fax: +44 (0)114 222 5943.
E-mail address: n.c.hyatt@sheffield.ac.uk (N.C. Hyatt).

0022-3115/$ - see front matter © 2013 The Authors. Published by Elsevier B.V. All rights reserved.
http://dx.doi.org/10.1016/j.jnucmat.2013.08.019

1. Introduction

1.1. Background

A significant proportion of the UK higher activity radioactive waste inventory comprises Plutonium Contaminated Material (PCM), the untreated packaged volume of such wastes is projected to be in excess of 20,000 m^3 on the Sellafield site alone [1]. PCM wastes are generally packaged in PVC bags and stored in 200 L drums. The current treatment option for these wastes is super-compaction of the 200 L drums, with the resulting pucks stacked in 500 L containers and encapsulated with a cement grout. This approach is effective for the bulk of PCM waste arisings, however, there exists a significant quantity of non-compactable waste which requires additional treatment. Ideally, the selected treatment method for non-compactable PCM wastes should seek to immobilise long-lived Pu isotopes, which are radiotoxic and potentially mobile in the subsurface, within a passively safe material prior to interim storage and disposal [2]. There is growing interest in the use of thermal processes, such as vitrification, to treat PCM materials and other Intermediate Level Wastes (ILW[1]) which are incompatible with cement encapsulation [3–12]. Key drivers for the application of thermal treatment processes include the reduced volume, improved passive safety, and superior long term stability, of the vitrified wasteform products. These benefits are derived from oxidation of the metallic waste fraction, destruction of organic components, and evaporation of entrained water, combined with simultaneous immobilisation of radioactive and chemotoxic elements within a glass or slag (i.e. a partially crystallised glass) material; a separate metal phase may also be produced, which may assist in scavenging less electropositive (and potentially volatile) metals, such as Tc and Ru, if present. The objective is generally to achieve a product of low porosity, with the desired partitioning of radioactive and chemotoxic elements between glass and ceramic phases, and a homogeneous distribution of radionuclide host phases over the volume of the product wasteform. A review of the development and application of thermal treatment technologies to higher activity wastes in the UK, including potential technology platforms, was recently published by Hyatt and James [12]. In this contribution we demonstrate that simulant UK PCM wastes can be effectively treated by vitrification using additions of ground granulated blast-furnace slag (itself a waste product of steel manufacture).

1.2. PCM waste simulants

Four distinct PCM waste simulants were used in this study: PVC waste; metallic waste; masonry waste; and mixed waste (comprising all three aforementioned components). These four simulants represent bounding cases for PCM wastes arising on the Sellafield site. PCM wastes are contained in 200 L sealed mild steel drums, each weighing 20 kg and packed with 25–80 kg of PCM [2], see Fig. 1. The desired approach is to treat each drum in its entirety, using a common methodology, without repackaging of the content. Therefore, all waste simulants contain a significant mild steel component representative of the containment drum. The compositions of the four PCM waste simulants are given in Table 1, the compositions of the individual waste stream components are given in Table 2.

1.3. Plutonium content and choice of surrogate

The upper PuO_2 content of the PCM wastes is estimated to be 230 g Pu per 80 kg drum, equivalent to 0.32 wt% PuO_2 [2]. Since this study was concerned with demonstration of the proposed approach, CeO_2 was used as a surrogate for PuO_2, on grounds of safety, cost and expediency. We acknowledge that such a simulant cannot fully reproduce the physical and chemical behaviour of another element. However, Ce is amongst the most useful and representative inactive Pu simulants, albeit with limitations including different redox potentials [13,14]. Nevertheless, the solubility of trivalent Ce and Pu was found to be broadly similar in (boro)silicate glass compositions at temperature >1400 °C, relevant to the process conditions of this investigation [14]. The upper estimated PuO_2 content of PCM wastes is the molar equivalent of 0.207 wt% CeO_2. In the present study, we elected to use ca. five times the amount of CeO_2 surrogate, allowing for both conservatism in the approach (effectively representing the highest conceivable PuO_2 content) and to assist detection and quantification by analytical methods (particularly XRF and SEM/EDS). Thus, all melts were doped with 1.043 wt% CeO_2 as a PuO_2 surrogate.

Fig. 1. Storage of 200 L drums of PCM waste at the Sellafield site, UK.

1.4. Wasteform and process formulation

From consideration of the four PCM waste types in Table 1, and the objective of treating all waste types using a single methodology, it was considered that the high metal content required a mixed metal and oxide slag wasteform, since complete oxidation of the reactive metal waste fraction was unrealistic in the absence of an oxidising gas sparge. The presence of an oxide slag phase during processing was considered essential, in order to accommodate Pu/Ce which are largely insoluble in steels [15–17]. To maximise volume reduction, and assist partitioning of Pu/Ce into the slag fraction, both metal and slag phases were required to be fully molten during processing. The temperature-limiting factor in this requirement was the need to ensure that all steel components were fully molten during processing. The Fe–C phase diagram, the Fe–Cr–C phase diagram, and modified Ni-bearing versions thereof, all show that the liquidus temperature, T_{liq}, varies from ca. 1548 °C for pure Fe to ca. 1150 °C at 4.3 wt% C, increasing with further increase in C content [18–21]. The effects of Cr and Ni upon these upper and lower values of T_{liq} are generally small by comparison. Therefore, we selected 1560 °C as the target melting temperature, which was indeed sufficient to melt the steel components.

1.5. Slag wasteform fraction

In the case of PVC and metal wastes, no oxide or "slagging" materials were themselves available in the waste materials to

[1] The term ILW is used in the UK to describe those higher activity wastes (4GBq α-activity or 12 GBq β,γ-activity, per tonne) that are not sufficiently heat generating for this to be taken into account in the design of storage or disposal facilities.

Table 1
Representative inactive PCM waste simulants (laboratory Pyrex-type borosilicate glass assumed).

Waste type	PVC waste	Metal waste	Masonry waste	Mixed waste
Description	Drum and PVC	Drum, PVC, and metal	Drum, PVC and masonry	Drum, PVC, metal, and masonry waste
Mild steel (wt%)	44.44	20.00	30.00	30.00
PVC (wt%)	55.56	10.00	10.00	10.00
Metal items (wt%)	0	70.00	0	15.00
Masonry waste (wt%)	0	0	60.00	40.00
Glass (wt%)	0	0	0	5.00
Total	100.00	100.00	100.00	100.00

Table 2
List of individual PCM waste components.

PCM waste component	Constituent	Weight %
Metal items	18/8 Stainless steel	95.494
	Aluminium	0.990
	Copper	0.495
	Lead	1.979
Masonry waste	Masonry, crushed	94.009
	Window glass	4.948
PuO_2	CeO_2 surrogate	1.043

immobilise the Pu/Ce surrogate inventory. Since a primary requirement was that all waste types should be treated using the same methodology, it was necessary to define a suitable oxide "slagging" additive and the proportion of additive to waste feed. The molten slag and metal fractions are required to be in equilibrium during the vitrification process, therefore, we selected Ground Granulated Blast-furnace Slag (GGBS) as the additive. GGBS is essentially a $CaO–Al_2O_3–SiO_2$ glass, produced as waste product from steel making [22,23]. GGBS is a low cost and commercially-available material, typically >99% amorphous by volume. Glasses in the $CaO–Al_2O_3–SiO_2$ system, have capacity for substantial incorporation of other elements present in the PCM wastes, particularly FeO_x (up to ca. 40 wt%) and PuO_2 (up to ca. 20 wt%), and are known to exhibit high chemical durability [24–26]. Furthermore, GGBS could be expected to be compatible with the aluminosilicate and calcium aluminosilicate building wastes present in the masonry and mixed PCM waste types, allowing all four waste types to be treated with the same additive. Initial scoping experiments confirmed the suitability of using GGBS as an additive, with a 1:1 ratio of waste to additive by weight. In an effort to minimise the amount of additive used, and hence maximise waste loading potential, a 3:1 ratio of waste to additive was used for the research reported here.

1.6. Metallic wasteform fraction

The metallic PCM waste components, given in Tables 1 and 2, suggest that this fraction of the vitrified PCM wastes should consist predominantly of a carbon steel, except in the case of metal waste feed, for which a high Ni Cr steel incorporating trace Al, Pb and Cu could be expected. No additions to improve performance or capability of the metal wasteform fraction were considered necessary (for example, additions of Zr in an effort to incorporate Pu in intermetallics as noted by Keiser and Abraham [16,17]), since the aim was to effectively partition Pu/Ce into the slag fraction. This could potentially allow the metallic fraction to be disposed of as LLW, licenced waste, or even reused, thus drastically reducing the volume of higher activity waste requiring storage or disposal, leading to substantial life cycle cost savings. It should be noted, however, that *in operando* tapping of liquid slag and metal, to achieve separation of these components, has not yet been routinely demonstrated using currently available thermal treatment technologies. Post process separation of slag and metal components would not be desirable, since the primary aim of the thermal treatment process is to produce a packaged product suitable for interim storage and disposal.

2. Experimental procedures

2.1. Simulant PCM waste preparation

The four bounding PCM wastes, given in Table 1, were simulated using the most appropriate materials and geometries. "Mock up" PCM drums were assembled using the following components: PCM drums were simulated using mild steel paint cans and lids (Fenton Packaging Ltd.); PVC bags were replicated using identical PVC sheeting (Romar Workwear Ltd.); the metallic waste was simulated using commercial grade 18/8 stainless steel, aluminium and copper (Avus Metals & Plastics Ltd.), and lead shot (Aldrich); the inorganic waste was simulated using waste Pyrex labware, crushed masonry, concrete and window glass; CeO_2 (from Acros Organics, >99.9%; dried 15 h at 600 °C) was used as a PuO_2 surrogate. Commercially available ground, granulated blast-furnace slag "Calumite" was used as an additive [27]. The analysed chemical composition is given in Table 3. Calumite is a powdered material, with a typical particle size distribution between limits of ca. 40 to ca. 400 μm.

PCM waste simulants and additives were weighed according to the formulations shown in Table 4 (weight fractions of composite items are given in Table 2). As-prepared simulants are shown in Fig. 2. Can lids were pierced to allow PVC combustion and gas egress early in the thermal cycle, thereby avoiding potentially dangerous explosive releases. Waste cans were crushed slightly at the can base to allow good ingress into the containment crucible (Fig. 2e). The required quantity of GGBS was added down the sides and on top of each sealed PCM simulant can as shown in Fig. 2.

2.2. Thermal processing

Samples were melted using a waste to GGBS additive ratio of 3:1 in alumina crucibles. However, initial scoping studies indicated

Table 3
Composition of Calumite Ground Granulated Blast-furnace Slag (GGBS).

Component	Weight %
SiO_2	35.7
Al_2O_3	13.2
Na_2O	0.2
K_2O	0.4
MgO	8.8
CaO	39.7
Fe_2O_3	0.3
MnO	0.5
TiO_2	0.5
SO_3	0.8

Table 4
PCM simulants (actual weights used).

Weight (g)	PVC waste	Metal waste	Masonry waste	Mixed waste
Mild steel	40.05	40.16	40.19	40.28
Metal items	0	144.08	0	20.63
Masonry waste	0	0	81.84	54.68
Glass (Pyrex®)	0	0	0	6.84
PVC sheeting	51.20	20.52	13.65	13.7
CeO_2	0.963	2.1376	1.4247	1.4256
Sub-total	92.21	206.90	137.10	137.56
GGBS additive	30.70	68.98	45.78	45.87
Total weight	122.93	275.88	182.88	183.43

the metal waste feed to be incompatible with alumina crucibles, due to prohibitive corrosion, and "Salamander" Plumbago crucibles, formed from a clay/graphite composite, were preferred (supplied by Morgan Ceramics). Crucibles, containing simulant waste and additive, were placed in an electric muffle furnace and heated overnight at 2 °C/min to 1100 °C for 8 h; crucibles were subsequently transferred to a gas-fired furnace, which had been preheated to 1100 ± 25 °C, then ramped to 1560 ± 10 °C over a period of 90 min. The preheat step was necessitated by the requirement to avoid thermal shock of the alumina crucibles. Temperature measurements were verified using an optical pyrometer throughout the melting procedure. Crucibles were held at 1560 ± 10 °C for a total of 2.5 h, then removed from the furnace and allowed to cool in air. During the transfer of the preheated metal waste crucible, from the electric muffle furnace to the gas-fired furnace, it was noted that a small but significant amount of the slag phase had "foamed over" the top of the crucible likely due to partial oxidation of the clay/graphite crucible component (see Section 3.1).

2.3. Characterisation

2.3.1. Density measurements

The density of the each slag fraction was determined using He gas pycnometry on powdered materials in the size fraction between mesh sizes 100 (0.149 mm) and 200 (0.074 mm). An AccuPyc 1340 II pycnometer was used with 200 purges of the chamber, 50 cycles, an equilibration rate of 0.005 psi min^{-1} at 25 °C in a 1 cm^3 chamber and a fill pressure of 12.5 psi. The estimated precision was ±0.01 g cm^{-3}. The density of each metal fraction was determined using the Archimedes method in deionised water. Three separate measurements were averaged in each case. The estimated precision was ±0.02 g cm^{-3}.

2.3.2. Chemical analyses

Chemical analyses were performed by X-ray fluorescence (XRF) spectroscopy and Inductively Coupled Plasma Optical Emission Spectroscopy (ICP–OES); the chloride content in slag and metal

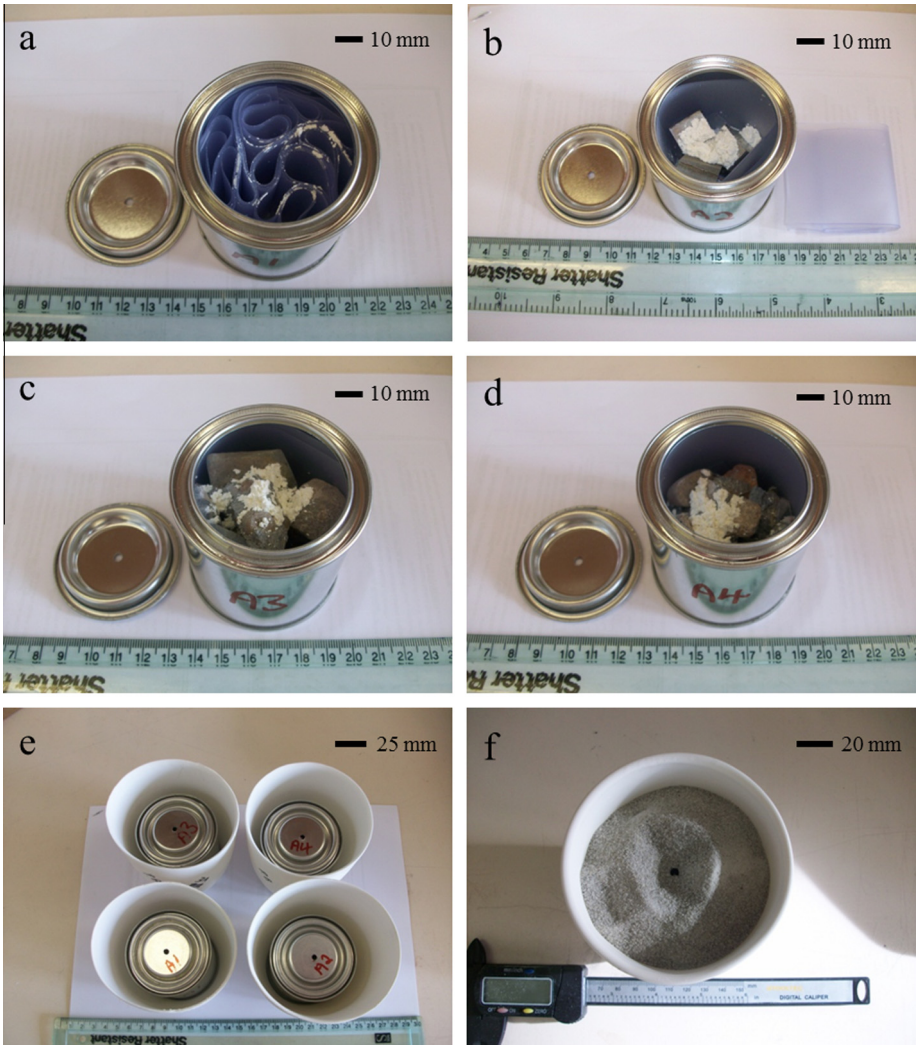

Fig. 2. Showing simulant PCM drum mock ups (a) PVC waste, (b) metal waste, (c) masonry waste, (d) mixed waste, (e) mock ups in alumina crucibles, and (f) addition of GGBS to assembled mock up.

products was determined by a standard addition method using samples dissolved in a mixture of hot HNO_3 and HBF_4. ICP–OES analysis of Ce content at 100–1000 ppm was associated with a relative uncertainty of 5% based on analysis of uniform reference materials. At 10–100 ppm of Ce, the relative uncertainty increased to 20%, and below 10 ppm the relative uncertainty was 30%. Errors associated with XRF analyses are given in the relevant tables.

2.3.3. Scanning electron microscopy with energy-dispersive X-ray spectroscopy

Scanning electron microscopy (SEM) with energy-dispersive X-ray spectroscopy (EDS) and Secondary Electron Imaging (SEI) and/or Backscattered Electron Imaging (BEI) was carried out primarily with a JEOL JSM6400 SEM and Oxford Instruments EDS. Specimens were prepared by mounting representative samples in epoxy resin, curing, grinding using successive grit SiC papers to 1200 grit, and polishing using diamond paste to 1 μm grade. Specimens were carbon coated prior to SEM analysis.

2.3.4. X-ray diffraction

X-ray diffraction was performed on powdered (<75 μm) samples of glass and pieces of metal, using a Siemens D5000 goniometer with Co K radiation and a diffracted beam monochromator. Analyses of the resulting diffraction patterns were performed using the WinXPoW software package.

2.3.5. Dissolution in simulated hyperalkaline conditions of a Geological Disposal Facility

Dissolution experiments were based on a modification of ASTM C1285-02 (2008) Product Consistency Test (PCT) Test Method B [28], for a full description of the methodology the reader is referred to the work of Utton et al. [11]. The slag wasteform fractions were prepared by grinding in a Tema mill, the fraction between mesh sizes 100 (0.149 mm) and 200 (0.074 mm) was collected, washed in ASTM Type I water and isopropanol (using an ultrasonic bath), and dried overnight at 90 °C. The test was carried out in triplicate for each sample and a blank (in duplicate) was carried throughout the procedure. Experiments were carried out under dry nitrogen and all solutions were made in de-aerated ASTM Type I water at 50 °C, to avoid carbonation and precipitation of calcium carbonate. The wasteform samples were weighed into the HDPE vessels and saturated calcium hydroxide solution was added (to simulate the hyperalkaline conditions of a UK cementitious Geological Disposal Facility (GDF)). The ratio of slag wasteform surface area to solution volume (SA/V) was 1200 m^{-1}. The mean particle diameter was assumed to be 112 μm [28], and the number of particles was calculated from pycnometry density measurements. In an effort to maintain saturation of the calcium hydroxide solution, an ultrafiltration unit filled with calcium hydroxide slurry, was suspended in the solution. The vessels were sealed and placed in an oven at 50 °C. The solutions were sampled after 3, 7, 14, 21 and 28 days and the vessels were returned to the oven after sampling. Aliquots were withdrawn from each vessel and passed through a 0.2 μm syringe filter to remove particulates. The solutions were then acidified with concentrated nitric acid (10 μl per ml). The total amount of solution removed was less than 10% of the original volume. The leachate was analysed by ICP Mass Spectroscopy, except for Na and K which were determined by Atomic Emission Spectroscopy.

2.3.6. Ce L_3 edge X-ray Absorption Spectroscopy (XAS)

Ce L_3 edge XAS data from all slag fractions, plus CeO_2, and $CePO_4$ (with the monazite structure) were acquired on beamline X23A2 of the National Synchrotron Light Source (NSLS), Brookhaven National Laboratory (BNL), USA. This beamline is configured with a piezo-feedback stabilised Si (311) upwards reflecting monochromator and single bounce harmonic rejection mirror. Data for CeO_2 and $CePO_4$ were acquired in transmission mode using finely ground specimens dispersed in BN to achieve a thickness of one absorption length. For the slag fraction specimens, data were acquired in fluorescence mode. Incident and transmitted beam intensities were measured using ionization chambers operated in a stable region of their I/V curve filled with mixtures of He and Ar or N_2. Fluorescence emission was detected using a four channel Si-drift detector, with appropriate dead time correction as described previously [29]. Data reduction and analysis was performed using the program Athena [30].

3. Results

3.1. Melting behaviour and appearance

The observed melting behaviour generally showed that the last items to melt were, as expected, the steel components. No violent reactions were observed between the waste simulants and glass additive. However, the alumina and clay/graphite crucibles suffered obvious corrosion during melting. In the case of samples melted in alumina crucibles, this resulted in the slag fraction of the wasteform having a content of Al_2O_3 greater than the nominal composition (see Section 3.2). In the case of samples melted in the clay/graphite crucibles, both slag and metal fractions were found to contain carbon derived from crucible corrosion (see Section 3.4). In addition, the clay/graphite crucibles exhibited significant weight loss due to oxidation at high temperature. Sample appearances varied considerably as a function of the PCM waste type, as shown in Fig. 3. A substantial metallic wasteform fraction resulted for the vitrified metal waste type, whereas only a small metal component was obtained in the mixed waste type. In contrast, the vitrified PVC and masonry waste types appeared to be composed only of slag material with no appreciable fraction of metallic component. The slag derived from the metal waste feed exhibited little obvious texturing or visible crystallinity. In contrast, the slag fraction derived from the masonry waste consisted of an upper glassy layer and a lower crystalline layer, and the slag fractions derived from the PVC and mixed wastes were, respectively, partially and strongly crystalline throughout.

3.2. Composition of slag and metallic wasteform fractions

The XRF determined compositions of major elements in the slag and metallic wasteform fractions are reported in Tables 5 and 6, respectively, together with Ce determined by ICP–OES. Ce was determined to be effectively partitioned to the slag fraction, as expected. The overriding difference in slag fraction composition is the Fe_2O_3 content of the final oxide fraction of the wasteform; this is apparently dominated by the type of crucible used and therefore by the degree of oxidation available to the (waste plus additive) mixtures during the thermal treatment process. The higher Fe_2O_3 content in the slag fraction of the PVC waste, compared to that derived from masonry and mixed waste types, is a consequence of the proportionately higher mild steel component. The slag resulting from the metal waste type, melted in a clay/graphite crucible, has a very low Fe_2O_3 content consistent with partitioning of Fe into the substantial metal fraction under reducing conditions. Chemical analysis determined no measurable retention of Cl within the slag fraction of the wasteforms. It was therefore concluded that all Cl present in the PVC was volatilised by the high temperature treatment. Analyses of the metallic fractions were consistent with the composition of the wastes from which they originated.

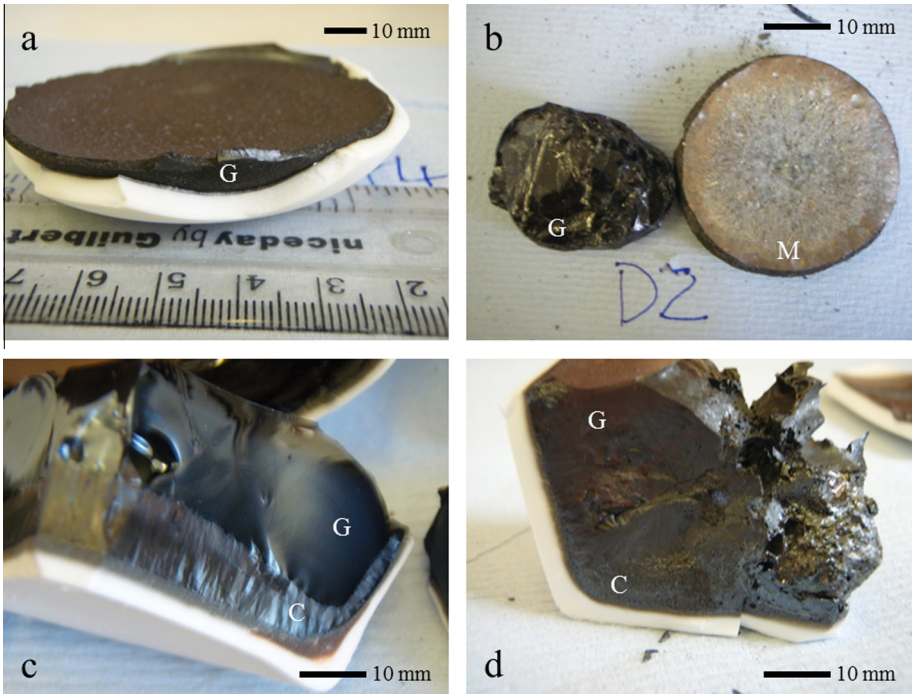

Fig. 3. Showing vitrified simulant PCM drum mock ups (a) PVC waste, (b) metal waste, (c) masonry waste, and (d) mixed waste, the glass (G) and crystalline (C) components of the slag fraction, and metallic fraction (M) are labelled.

Table 5
Composition of slag wasteform components determined by XRF, except Ce determined by ICP–OES; measured Cl content <100 ppm.

Component (wt%)	PVC waste	Metal waste	Masonry waste	Mixed waste
Na_2O	0.13 ± 0.02	0.38 ± 0.03	0.39 ± 0.03	0.41 ± 0.05
MgO	2.15 ± 0.09	4.28 ± 0.12	2.17 ± 0.09	2.03 ± 0.09
Al_2O_3	21.22 ± 0.26	16.53 ± 0.24	18.7 ± 0.26	16.77 ± 0.24
SiO_2	14.8 ± 0.23	52.45 ± 0.44	37.94 ± 0.38	34.46 ± 0.35
P_2O_5	0.47 ± 0.05	<0.05	0.20 ± 0.03	0.18 ± 0.03
K_2O	0.08 ± 0.02	0.41 ± 0.05	0.36 ± 0.03	0.15 ± 0.03
CaO	16.28 ± 0.24	18.26 ± 0.26	12.1 ± 0.24	13.73 ± 0.23
TiO_2	0.24 ± 0.03	0.87 ± 0.06	0.27 ± 0.03	0.20 ± 0.03
Mn_3O_4	0.32 ± 0.03	1.62 ± 0.08	0.24 ± 0.03	0.46 ± 0.05
Cr_2O_3	0.07 ± 0.02	1.68 ± 0.08	0.05 ± 0.02	2.09 ± 0.09
Fe_2O_3	41.51 ± 0.39	1.32 ± 0.06	26.88 ± 0.31	28.10 ± 0.32
ZrO_2	<0.05	<0.05	0.32 ± 0.03	0.39 ± 0.03
ZnO	<0.05	<0.05	<0.05	<0.05
BaO	1.06 ± 0.06	0.92 ± 0.06	0.48 ± 0.05	0.54 ± 0.05
SrO	<0.05	0.05 ± 0.02	<0.05	<0.05
CuO	0.01 ± 0.02	0.03 ± 0.02	0.03 ± 0.02	0.09 ± 0.02
PbO	<0.005	<0.005	<0.005	0.02 ± 0.02
Ce_2O_3	1.53 ± 0.06	1.36 ± 0.06	0.67 ± 0.03	0.78 ± 0.03
SUM	99.56 ± 0.60	98.53 ± 0.60	100.55 ± 0.60	99.94 ± 0.60

3.3. Densities of optimised PCM wasteforms

Table 7 reports the measured densities of the slag and (where formed) metallic fractions of the PCM wasteforms. The densities of the measured metallic fractions are consistent with the compositions of steels and high iron alloys [31].

3.4. Phase analysis and microstructure

3.4.1. PVC waste

The slag fraction was found to be composed of a $CaO–Fe_2O_3–Al_2O_3–SiO_2$ glass, plus crystalline $Ca_2(Mg_2Fe_4)(Al_4Si_2)O_{20}$ (dorrite), $(Mg,Fe)(Cr,Fe,Al)_2O_4$ (spinel), and at least one other unidentified phase; see Figs. 4 and 5. EDS analyses showed Ce (measured as Ce_2O_3) to be concentrated primarily in the glass phase (4.04 wt%) compared to the crystalline phases (0.43 wt%).

3.4.2. Metal waste

The slag fraction of this sample was found to be largely composed of a $CaO–Fe_2O_3–Al_2O_3–SiO_2$ glass, with small inclusions of graphite (resulting from crucible corrosion) and Fe (with trace Ni and Cr); see Figs. 6 and 7 (note: the volume fraction of the metallic inclusions was below the detection limit of X-ray diffraction). SEM and EDS mapping showed the metallic fraction to be composed of a major Fe bearing phase containing Si and Ni, a minor Fe and Cr bearing phase, and trace amounts of and C (derived from crucible corrosion), see Fig. 8. EDS analysis demonstrated Ce to be concentrated exclusively within the glass phase, within detection limits.

Table 6
Composition of metal wasteform components determined by XRF in wt%; except Ce determined by ICP–OES.

Component (wt%)	Metal waste	Mixed waste
Al	0.05 ± 0.02	0.11 ± 0.02
Si	1.95 ± 0.09	0.23 ± 0.05
Ti	<0.05	<0.05
V	0.06 ± 0.02	<0.05
Cr	10.42 ± 0.20	3.08 ± 0.11
Mn	0.43 ± 0.05	<0.05
Fe	74.68	80.62
Co	0.18 ± 0.03	0.26 ± 0.03
Ni	7.76 ± 0.17	11.12 ± 0.20
Nb	<0.05	<0.05
Mo	1.52 ± 0.08	2.45 ± 0.09
Sn	0.06 ± 0.02	0.09 ± 0.02
W	0.09 ± 0.02	0.13 ± 0.03
Cu	0.64 ± 0.05	0.45 ± 0.05
Pb	<0.001	0.013 ± 0.02
Ce	0.014 ± 0.003	0.019 ± 0.004
SUM	97.85 ± 0.60	98.57 ± 0.60

Table 7
Archimedes and pycnometry densities of optimised PCM wasteforms.

Sample	Density (g cm^{-3})
PVC waste: slag fraction	3.76 ± 0.01
Metal waste: slag fraction	2.80 ± 0.01
Masonry: slag fraction	3.16 ± 0.01
Mixed waste: slag fraction	3.35 ± 0.01
Metal waste: metal fraction	7.55 ± 0.02
Mixed waste: metal fraction	7.03 ± 0.02

3.4.3. Masonry waste

Powder XRD and SEM/EDS demonstrated the slag fraction to be composed of a $CaO–Fe_2O_3–Al_2O_3–SiO_2$ glass and a crystalline $(Mg,Fe)(Cr,Fe,Al)_2O_4$ (spinel) phase; see Figs. 9 and 10. The XRD reflections of the spinel phase exhibited noticeable broadening consistent with the small (<1 μm) particle size evident in the SEM images. EDS analyses showed Ce (measured as Ce_2O_3) to be concentrated primarily in the glass phase (0.90 wt%) compared to the crystalline phases (0.21 wt%).

3.4.4. Mixed waste

The slag fraction of this sample was found to be a $CaO–Fe_2O_3–Al_2O_3–SiO_2$ glass, plus crystalline $Ca(Mg,Al)(Si,Al)_2O_6$ (diopside), $(Mg,Fe)(Cr,Fe,Al)_2O_4$ (spinel), and at least one other unidentified phase; see Figs. 11 and 12. Again, the XRD reflections of the spinel phase exhibited noticeable broadening consistent with the small (<1 μm) particle size evident in the SEM images. SEM and EDS mapping showed the metallic fraction to be composed of a major Fe bearing phase with minor Ni and Cr, the glass/metal interface was defined by a chromium oxide phase; see Fig. 13. EDS analyses showed Ce to be concentrated exclusively in the glass phase, no Ce was found in the metallic fraction within detection limits.

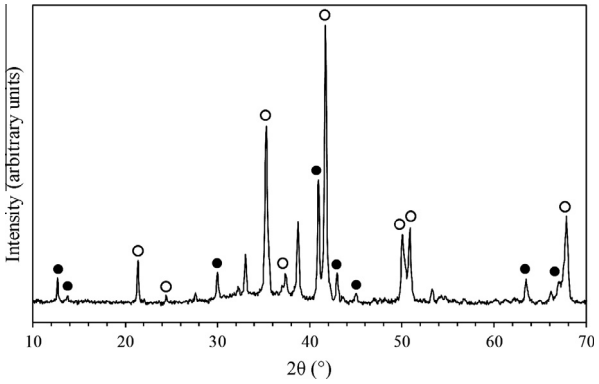

Fig. 5. X-ray powder diffraction pattern showing identified reflections corresponding to dorrite $Ca_2(Mg_2Fe_4)(Al_4Si_2)O_{20}$ (filled circles) and spinel $(Mg,Fe)(Cr,Fe,Al)_2O_4$ (open circles) phases, together with diffuse scattering corresponding to the presence of an amorphous component, in the slag produced by vitrification of PVC waste type. Unlabelled reflections correspond to unidentified phase(s).

3.5. Dissolution in simulated hyperalkaline conditions of a cementitious Geological Disposal Facility

The average pH of the blank and all test solutions was found to be constant at 12.2 ± 0.1 units over the duration of the dissolution experiments, demonstrating the solution pH to be effectively buffered over the test period. Fig. 14 shows the concentration of Ca in the blank and test solutions, as a function of time. Within precision, the concentration of Ca in the blank solution remained effectively constant at 0.8 ± 0.1 g L^{-1} over the 28 day test period. In all test solutions, however, the Ca concentration showed a smooth decrease with time, reaching 0.4 ± 0.1 g L^{-1} after 28 days. The effectively constant Ca concentration in the blank solution is consistent with the exclusion of CO_2 under the anoxic conditions of the experiment, which would otherwise lead to carbonation and precipitation of $CaCO_3$. Consequently, the depletion of Ca from solution in the case of the test experiments implies the precipitation of Ca bearing secondary alteration phases at a rate which exceeds the diffusion of Ca into solution from the filter unit. A similar depletion of Ca in solution was reported from experiments on other simulant ILW glasses under similar conditions by Utton et al. [11].

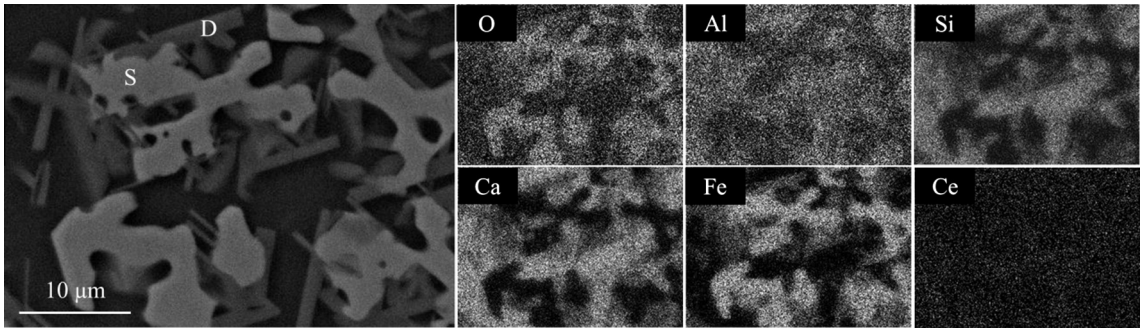

Fig. 4. BSE image and EDS maps showing microstructure of slag produced by vitrification of PVC waste type and partitioning of key elements between crystalline and glass components; crystalline spinel (S) and dorrite (D) phases are highlighted – see Fig. 5.

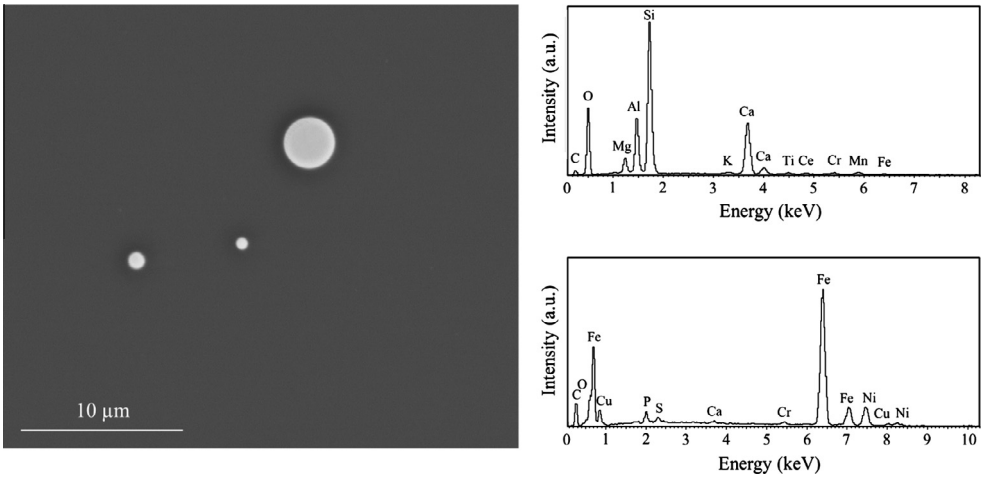

Fig. 6. BSE image and EDS data showing microstructure and composition of slag fraction (with metallic inclusions) produced by vitrification of metal waste type; top EDS spectrum corresponds to grey matrix phase, bottom EDS spectrum corresponds to bright spherical inclusions.

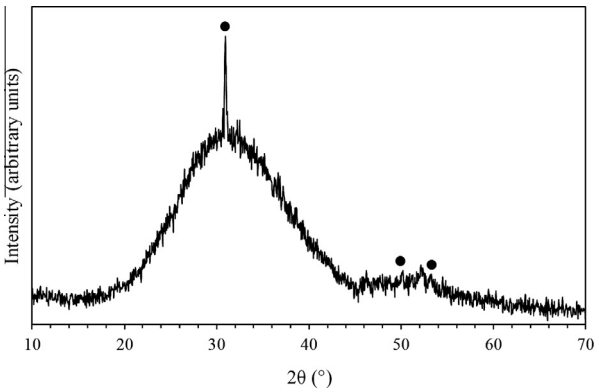

Fig. 7. X-ray powder diffraction pattern showing identified reflections corresponding to graphite (filled circles), together with diffuse scattering corresponding to the presence of an amorphous component, in the slag fraction produced by vitrification of metal waste type.

The compositions of PCM slag simulants did not contain any significant quantity of boron or lithium, which are normally used as a soluble marker of glass dissolution since these elements do not generally participate in the precipitation of secondary alteration products. Therefore, the normalised mass loss of Na and K, shown in Fig. 15, were considered as a marker for slag dissolution.

The normalised mass loss of Na and K was similar for the slag materials derived from vitrification of the mixed, masonry and metal wastes, as shown in Fig. 15. Measured values of NL_{Na} and NL_K were observed to increase rapidly over the first 14 days of the experiment; thereafter, NL_{Na} and NL_K increased more slowly and appeared essentially constant after 28 days. However, experiments of longer duration are required to confirm this conclusion. The normalised mass loss of Si was also similar for the slag materials derived from vitrification of the mixed, masonry and metal wastes, as shown in Fig. 15. Within precision, the measured NL_{Si} values were unchanged over the 28 day test period, however, as shown in Fig. 15, a gradual upward trend in NL_{Si} was apparent over the course of the experiments. The concentration of Si in test solutions after 28 days was 0.07–0.15 mg L^{-1}, significantly below, but approaching, the estimated silica saturation limit under the conditions of the experiment (ca. 0.3 mg L^{-1}, estimated using PHREEQC [32]). These observations suggest that the apparent steady state conditions are controlled both by the formation of a calcium silicate phase (depleting Ca from solution) and the approach to silica saturation.

The normalised mass loss of Na, K and Si for the slag material derived from vitrification of the PVC waste, was evidently greater than that from that of the other slag materials, as shown in Fig. 15. The rate of normalised mass loss of Na and Si decreased rapidly after the first 14 days of the experiment, suggesting the approach to pseudo steady state conditions. The concentration of Si in

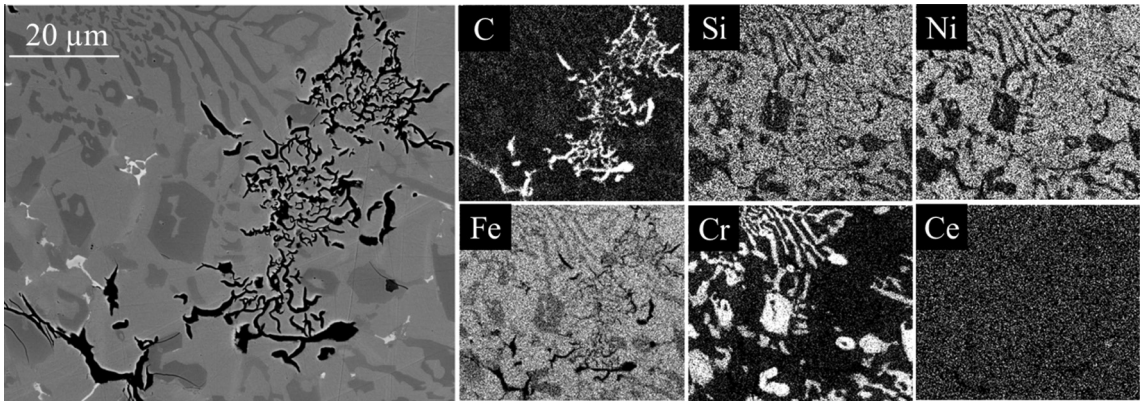

Fig. 8. BSE image and EDS maps showing microstructure of metal fraction produced by vitrification of metal type waste and partitioning of key elements.

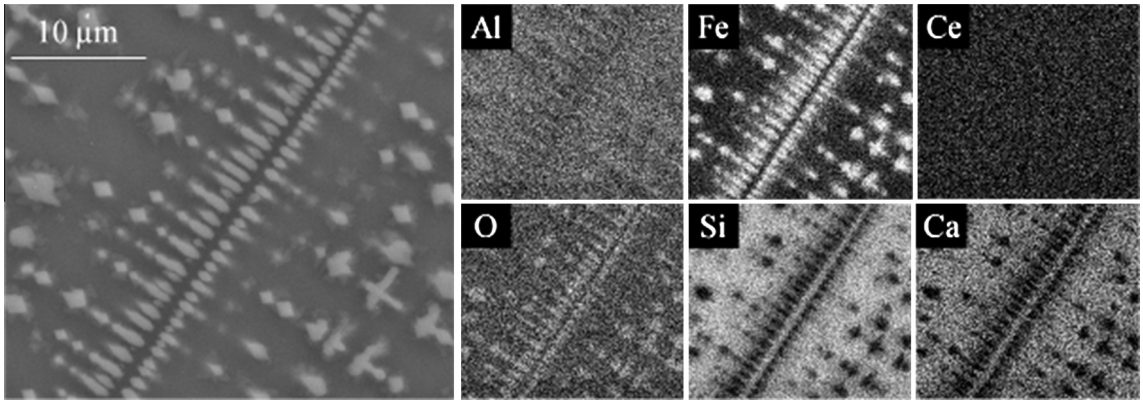

Fig. 9. BSE image and EDS maps showing microstructure of slag fraction produced by vitrification of masonry waste type and partitioning of key elements between crystalline and glass components.

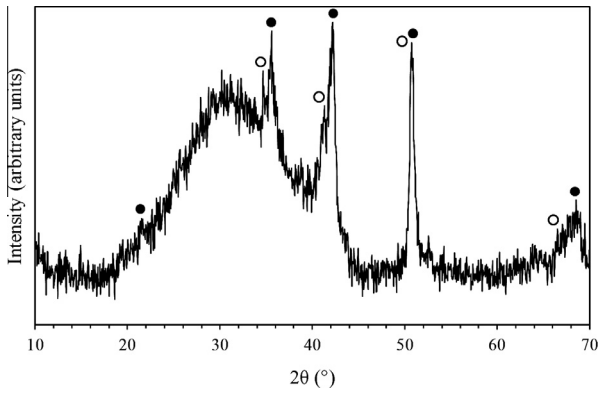

Fig. 10. X-ray powder diffraction pattern showing identified reflections corresponding to two distinct $(Mg,Fe)(Cr,Fe,Al)_2O_4$ (spinel) phases (highlighted by closed and open circles), together with diffuse scattering corresponding to the presence of an amorphous component, in the slag produced by vitrification of masonry waste type.

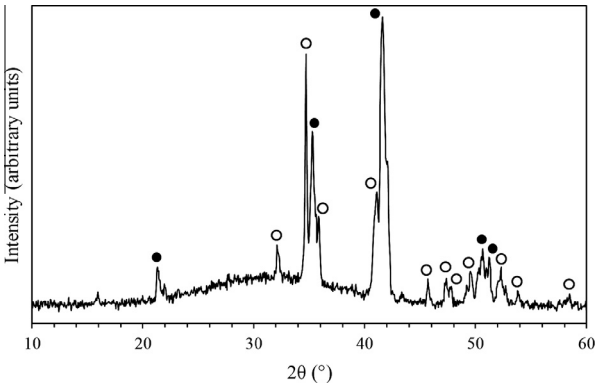

Fig. 12. X-ray powder diffraction pattern showing identified reflections corresponding to diopside $Ca(Mg,Al)(Si,Al)_2O_6$ (open circles) and spinel $(Mg,Fe)(Cr,Fe,Al)_2O_4$ phase (filled circles), together with diffuse scattering corresponding to the presence of an amorphous component, in the slag produced by vitrification of mixed waste type. Unlabelled reflections correspond to unidentified phase(s).

solution at 28 days was close to the estimated saturation limit, suggesting that the observed decrease in the rate of glass dissolution is due to the approach to silica saturation.

In summary, the PVC derived slag was apparently less durable than the other slag materials, under the test conditions applied. The durability of the slag materials derived from mixed, masonry and metal wastes, increased in this order, but were broadly similar. The concentration of Ce in solution was below or close to the detection limit over the 28 day test period and did not exceed $0.4\ \mu g\ L^{-1}$, consistent with the low solubility of trivalent lanthanides at high pH, as discussed in Section 4.3.

3.6. Determination of Ce oxidation state by Ce L_3 edge XAS

X-ray Absorption Spectroscopy has been shown to be a powerful tool for the investigation of element speciation and local co-ordination in (boro)silicate glasses for radioactive waste immobilisation [33–35]. Fig. 16 shows the Ce L_3 edge X-ray Absorption Near Edge Structure (XANES) of the slag fractions, together with

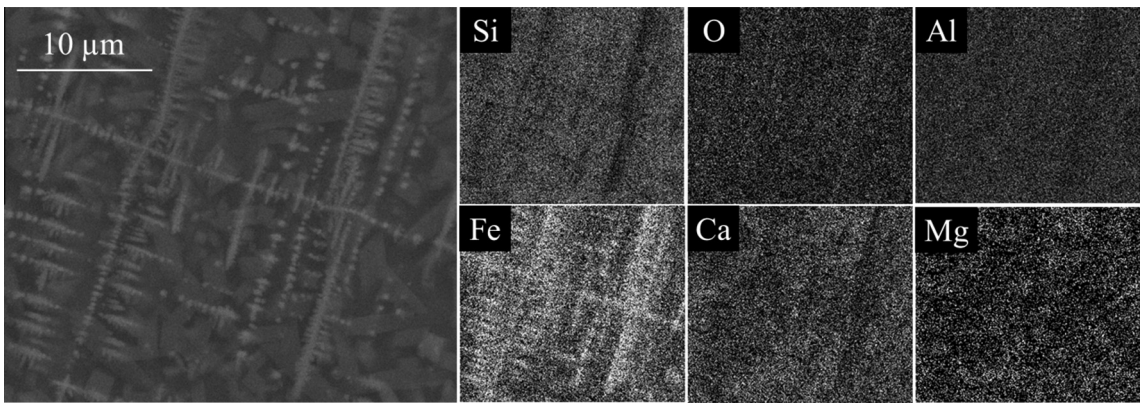

Fig. 11. BSE image and EDS maps showing microstructure of the slag fraction produced by vitrification of mixed waste type and partitioning of key elements.

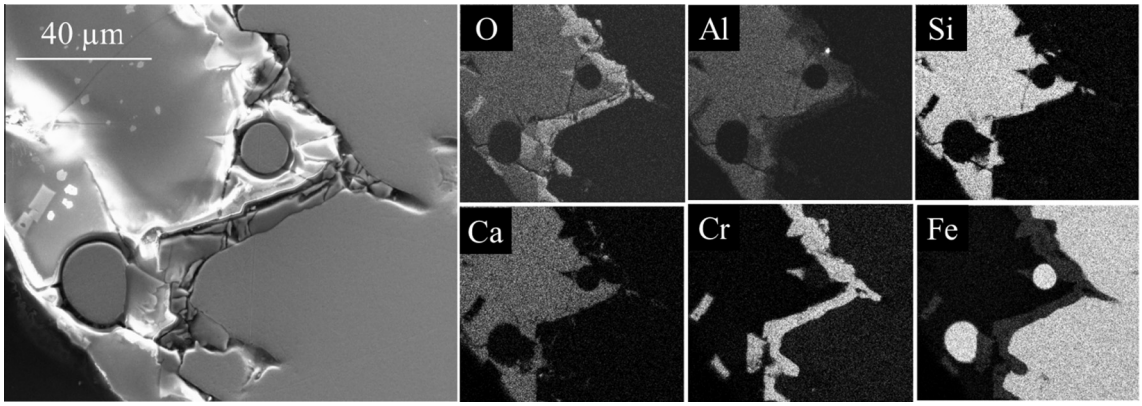

Fig. 13. BSE image and EDS maps showing microstructural interface between slag and metal fractions produced by vitrification of mixed waste type and partitioning of key elements.

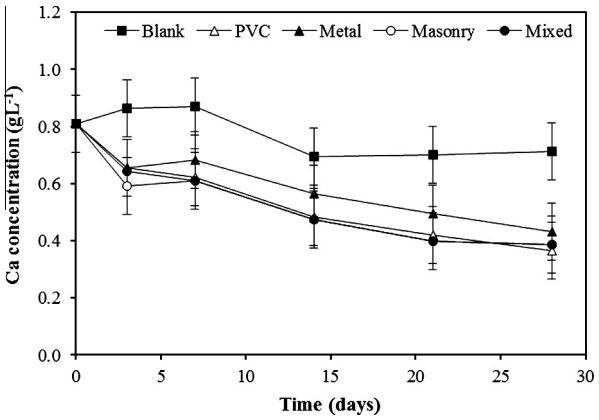

Fig. 14. Ca concentration in solutions of dissolution and blank experiments as a function of time.

the data acquired for CeO_2 and $CePO_4$ (monazite) standards. The Ce L_{III} edge XANES of Ce^{3+} (e.g. $CePO_4$) is characterised by a white line comprising a single intense feature attributed to the transition from an initial $2p^64f^15d^0$ state to a $2p^54f^15d^1$ final state, modified by local density of unoccupied states. In contrast, the Ce L_3 edge XANES of Ce^{4+} (e.g. CeO_2) is characterised by a white line comprising two features of lower relative intensity. Following the notation convention employed by Bianconi et al. [36], the consensus is that these two features, labelled A and B in Fig. 16, are due to transition from an initial $2p^64f^05d^0$ state to: (a) the $2p^54f^05d^1$ final state; and (b) the $2p^54f^15d^1\underline{L}^1$ final state (where $\underline{L}^n$ denotes a ligand hole) [36–40]. Other more subtle features are also observed. Feature C is considered to be associated with transition to a $2p^54f^25d^1\underline{L}^2$ final state, whereas the weak feature D is assigned to quadrupole transitions [37–40]. The XANES spectra shown in Fig. 16 permit straightforward fingerprinting of Ce oxidation state. From comparison of the spectra it is apparent that the XANES data of slag fraction closely resemble that of $CePO_4$, demonstrating that Ce^{3+} is the dominant species. From consideration of our measurement resolution (0.1 eV) in comparison with the edge shift associated with Ce^{3+} and Ce^{4+} oxidation states (~1.6 eV), we estimate the detection limit of Ce^{4+} in our measurements to be ~6%.

4. Discussion

4.1. Cerium partitioning

Cerium partitioning within the wasteform may be considered in terms of two key partitioning ratios:

- Ce (slag fraction):Ce (metallic fraction)
- Ce (amorphous slag fraction):Ce (crystalline slag fraction/s)

No relic or precipitated Ce, Ce_2O_3 or CeO_2 were detected in any sample following vitrification, indicating that it was dissolved fully within the wasteform. ICP–OES analyses of the slag and metallic fractions (where formed), confirmed that Ce was overwhelmingly incorporated in the slag fraction. The ICP–OES method has the higher accuracy for total Ce, so these analyses are considered for partitioning between slag and metallic fractions. For partitioning between glass and crystalline components of the slag fraction, spatially resolved EDS analyses were used. It should be noted that the interaction volume of electrons with the sample, coupled with other sources of error, leads to significant uncertainties in the derived partitioning ratios within the slag component, which should therefore be considered only indicative at low concentration.

4.1.1. Partitioning of cerium between the oxide and metallic fractions

Cerium contents (as elemental Ce) of the slag fractions were in the range 0.67–1.16 wt% whilst the metallic fractions contained 0.007–0.019 wt% (Tables 5 and 6). The slag to metal partitioning ratios, based on Ce ICP–OES analyses, were calculated as summarised in Table 8 and show that at least 97% of the analysed Ce was partitioned into the slag phase.

Although the proportion of Ce partitioned into the metal fraction is small, it is not negligible. Assuming similar Pu distributions, the partitioning achieved would not be sufficient to permit disposal of the metal waste fraction as low level waste (LLW). Nevertheless, the partitioning ratios obtained are encouraging and could potentially be optimised by extended high temperature reaction to assist Pu transfer from the metal to slag phase, and by judicious adjustment of the proportion of additive to waste and processing conditions. Furthermore, the above calculations may be taken as conservative if we consider the possibility that small amounts of slag fraction may have been occluded in, or otherwise contaminated, the metal samples analysed. This seems entirely plausible, given that clean separation of oxide and metallic components was neither attempted nor achievable with certainty. The measured Ce content of the metallic fraction could be accounted for entirely, if this material contained approximately 1 wt% of the slag material.

4.1.2. Partitioning of cerium within the oxide fraction

The slag fractions derived from the PVC, masonry and mixed waste types all exhibited a significant crystalline component. Ce partitioning between the amorphous and crystalline phases was found to be dependent on the nature and quantity of the crystalline phase(s) present. The slag derived from vitrification of PVC waste

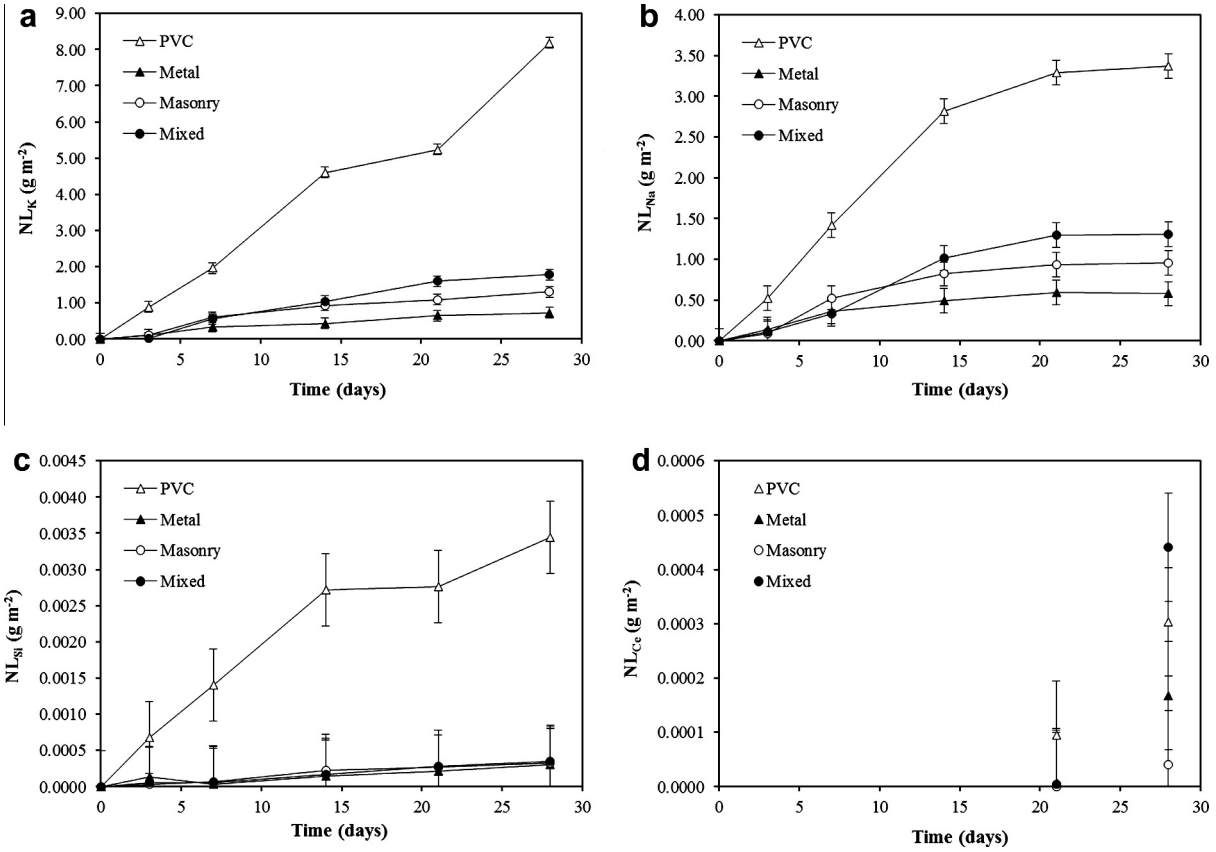

Fig. 15. Normalised mass loss of selected elements as a function of time in dissolution experiments: (a) K, (b) Na, (c) Si, and (d) Ce.

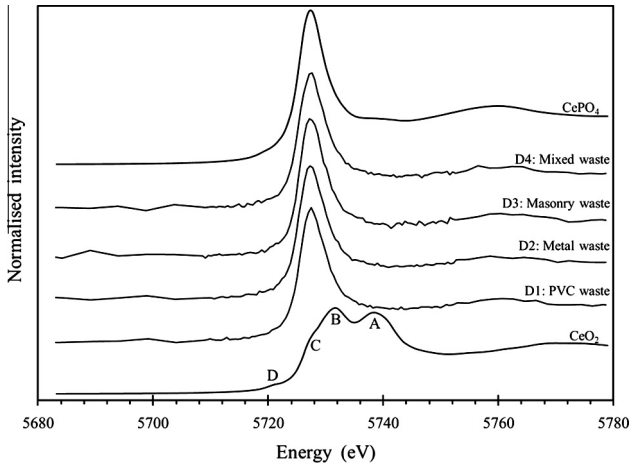

Fig. 16. Ce L_3 edge XANES data from CeO_2 (Ce^{4+} standard), $CePO_4$ (Ce^{3+} standard with the monazite structure), and slag fractions from vitrification of simulant PCM wastes; comparison of the position of the absorption edge and XANES features demonstrates the presence of Ce^{3+} in the slag materials.

exhibited a substantial crystalline component; consequently, the amorphous phase was enriched to ca. 4.0 wt% Ce_2O_3, but the accompanying dorrite and spinel phases incorporated low or trace levels of Ce_2O_3, ca. 1.0 and 0.2 wt%, respectively. The slag materials derived from vitrification of masonry and mixed wastes exhibited considerably smaller crystalline component, the amorphous phase contained ca. 1.2 wt% Ce_2O_3 with little or no detectable level of Ce in the accompanying crystalline phases. No crystalline phases were detected within the slag fraction derived from vitrification of the metal waste type. The dissolved Ce appeared to be homogeneously distributed throughout the amorphous matrix and no concentration gradients or cerium "hot spots" were apparent in EDS maps.

Table 8
Optimised sample cerium partitioning calculations based on ICP analyses.

Sample	Analysed Ce in slag (wt%)	Analysed Ce in metal (wt%)	Proportion of Ce analysed in slag phase (%)
Metal waste	1.16 ± 0.058	0.014 ± 0.0028	99
Mixed waste	0.67 ± 0.034	0.019 ± 0.0038	97

The upper analysed Ce_2O_3 content of 4.0 wt%, within the amorphous phase derived from the PVC waste, is equivalent to a Ce_2O_3 concentration of approximately 1.2 mol%. The solubility of Ce_2O_3 and Pu_2O_3 in (boro)silicate glasses has been shown to be broadly similar, with an upper limit of ca. 2 mol% at 1450 °C [14,41–43]. Therefore, it is considered feasible that the slag component of the wasteforms developed here could incorporate Pu at the concentrations expected. The solubility of trivalent Ce and Pu in silicate glasses is known to be significantly higher than that of tetravalent Ce and Pu, particularly above 1100 °C. Therefore, it may be understood that the strongly reducing conditions achieved in PCM vitrification effectively assist in the partitioning of Ce within the glass phase of the slag wasteform.

4.2. Dissolution behaviour in a simulated hyperalkaline GDF environment

The objectives of the preliminary dissolution experiments undertaken in this study were:

- To investigate compatibility with the hyperalkaline conditions expected in a cementitious UK GDF.
- To identify significant differences in the dissolution behaviour of the slag wasteforms in relation to their chemical composition in relation to the waste type.
- To compare the relative performance of the slag products with other vitrified ILW products considered potentially suitable for geological disposal.

The data reported here are consistent with the conclusions of a recently published study of model and full scale simulant ILW glass dissolution in saturated $Ca(OH)_2$ solution at 30–90 °C [9,11]. The observed depletion of Ca from solution has been shown to be associated with the formation of calcium silicate hydrate (CSH) phases, resulting from reaction between the hydrated glass surface and dissolved Ca [10,11,44]. This CSH phase has been shown act as a passivating layer at pH 8.7, reducing the rate of glass dissolution [44]. Although Ca was depleted from test solutions, the hyperalkaline pH, key to minimising the solubility of long lived actinides in the cementitious GDF concept [45], was maintained over the duration of the experiments, as discussed below.

The slag materials derived from metal, masonry and mixed wastes were found to be considerably more durable, compared to that derived from PVC waste, based on the normalised mass loss of Na, K and Si. In comparison to the other slag materials, the lower durability of PVC derived slag can be attributed to the low SiO_2 fraction in the glass as shown in Table 5 (due to the correspondingly high Fe_2O_3 content, as discussed in Section 3.1). Glass durability generally increases with increasing SiO_2 content in silicate glasses, as a consequence of the increasing ratio of bridging to non-bridging oxygens, leading to increased glass network polymerisation and reduced interconnectivity of alkali channels which permit exchange of cations between leachate solution and glass [46]. Likewise, the durability of the slag materials derived from mixed, masonry and metal wastes, increased in this order with increasing SiO_2 content, from 34 to 52 wt%, as shown in Table 5.

The initial and residual dissolution rates based on the normalised release of Na (measured over the first and final 7 days of the experiment, respectively) were 0.05 g m^{-2} d^{-1} and 0.002 g m^{-2} d^{-1} for the slags derived from metal, masonry and mixed wastes. These dissolution rates are comparable with the previously reported for simulant inactive UK ILW glasses, with initial and residual dissolution rates of 0.02–0.04 g m^{-2} d^{-1} and 0.003–0.005 g m^{-2} d^{-1}, respectively (based on NL_{Na} under similar conditions) [10,11]. The initial dissolution rate of the slag derived from PVC waste was markedly higher, ca. 0.2 g m^{-2} d^{-1}, as a consequence of the lower SiO_2 content of this glass. However, the residual rate of 0.01 g m^{-2} d^{-1} is comparable with that of other model and simulant full scale inactive UK ILW glasses.

Although Ca was depleted from test solutions, the hyperalkaline pH, key to minimising the solubility of long lived actinides in the cementitious GDF concept, was maintained over the duration of the experiments. Consequently, the measured Ce concentration in test solutions was generally below or close to the detection limit in test solutions up to 21 days and did not exceed 0.4 μg L^{-1}. Given the trivalent speciation of Ce relevant to this study, our findings are consistent with the reported solubilities of trivalent Pu, Am, Nd, Sm and La, which are lower than 0.5 μg L^{-1} at pH > 9 under inert (CO_2 free) atmospheres at 50–60 °C [47]. Ewart et al. and Berry et al. studied the solubility of several actinides in a cementitious near-field environment using saturated $Ca(OH)_2$ solutions under CO_2 free conditions [48,49]. Concentrations in solution of Pu^{4+} and Am^{3+}, the most relevant to this study, were reported to be below 0.02 μg L^{-1} at pH 12.

The corrosion behaviour of the metallic fractions of the PCM wasteforms was not investigated in this study, since the aim was to partition Ce, as the Pu surrogate, into the slag component (as was demonstrably achieved). However, a brief consideration is warranted as our results indicate that a small inventory of Pu may reside in the metallic fraction following thermal treatment. A detailed European study of metallic materials in GDF conditions by Kursten et al. [50] concluded that the current best estimates for corrosion rates of carbon steel in alkaline media are of the order of <0.12 μm y^{-1} at 30 °C, and <1 μm y^{-1} at 80 °C. If Pu is assumed to partition identically to Ce, this would translate to an estimated upper available Pu release inventory of 4×10^{-4} g m^{-2} d^{-1}.

In summary, it may be concluded that the slag materials produced from vitrification of the bounding PCM waste types considered, are broadly comparable, in terms of durability, to other simulant UK ILW glass products considered potentially suitable for geological disposal [10–12]. However, we cannot draw definitive conclusions concerning the compatibility of these wasteforms with a cementitious GDF concept, at the present time. To do so would require understanding and modelling of glass dissolution and solution reaction mechanisms that influence the pH buffering capacity of the backfill fluid, which is beyond the scope of the current study. Depletion of Ca from solution, as a consequence of reaction with the hydrated glass surface to form a calcium silicate hydrate (CSH) phase, may not necessarily be detrimental to the overall safety concept, since CSH materials are known to effectively sorb actinides from solution [51]. However, it is reasonable to conclude that the high durability of the PCM slags reported in this study, combined with the low solubility of actinides, under the hyperalkaline conditions of an ILW GDF, appear promising for application.

4.3. Volume reduction potential

Volume reduction is a key requisite for treatment of PCM: the untreated packaged volume on the Sellafield site alone is projected to be in excess of 20,000 m^3 [1]. The driver for maximum volume reduction, to minimise interim storage and disposal costs, does not impose a limit on volume reduction *a priori*. However, criticality concerns dictate that immobilised PCM requires a minimum level of dilution to ensure safe dispersion of Pu within the host matrix. This provides a lower boundary for the volume of vitrified PCM material. Further considerations of processing and GDF performance may provide additional constraints on volume reduction, but are out with the consideration of this study.

Relative to the untreated PCM waste, packaged in 200 L drums, the slags derived from vitrification of PVC and metal wastes achieved an estimated volume reduction of 95%, whereas the slags derived from vitrification of masonry and mixed wastes achieved an estimated volume reduction of 80%. These estimates, based on mass balance calculations, should be considered indicative rather than definitive, given the scale of the experiments and hence the sensitivity to small mass variations arising, for example, from: residual glass adhered to the crucible walls; corrosion of crucibles; foaming of glass melts; and, incomplete separation of slag and metal components.

As noted above, criticality considerations dictate lower boundaries for vitrified PCM volumes. Projected PuO_2 contents of PCM wastes are expected to have an average value in the region of 33 g Pu per 200 L drum, making an average of 0.165 g/L [52]. Criticality considerations dictate that the maximum allowable concentration of Pu is 60 g/L, and contingencies suggest that ideally a concentration of <6 g/L is preferable. If we assume that 6 g/L is a reasonable target for Pu concentration in the slag fraction, with 60 g/L an uppermost limit, it can be shown that, assuming one 200 L drum holds 230 g Pu, we require ca. 38 L of the slag fraction to accommodate Pu at a concentration of 6 g/L. This decreases to just 3.8 L of the slag fraction at the uppermost Pu concentration

limit of 60 g/L. This lower boundary for vitrified waste volume implies a maximum volume reduction factor of 98%. It may therefore be concluded that a 3:1 ratio of waste to GGBS, by weight, produces slag wasteform volumes commensurate with the preferred target concentration of Pu based on criticality considerations. However, lower waste to GGBS ratios, with a consequent increase in overall wasteform volume, may be preferable (particularly in the case of the PVC and metallic waste types), where estimated volume reduction may achieve Pu concentrations near the upper limit.

4.4. Comment on emissions to off gas system

Estimation of possible Pu release to the off gas system, based on the results of the vitrification melts carried out in this study, is made exceptionally difficult by the inaccuracy of the mass balance data concerning losses from the melt, especially given the relatively small size of the melts (<200 g) and significant crucible corrosion. Therefore, it is not possible to comment on the potential Pu release with confidence. Owing to the compositions of the Sellafield PCM wastes being vitrified (Tables 1 and 2; see also Ref. [2]), the greatest burden on the off-gas system in terms of volume will be provided by the combustion products of the PVC material. Less than 100 ppm of Cl were recorded in all samples, so it is likely that all of the Cl (as HCl) would be lost into the off-gas system. An additional burden will arise from any water present in the waste; carry-over and evaporation from the (additive + waste) mixtures being vitrified; and smaller quantities of SO_x, NO_x and oxides of carbon. Emission of toxic organic chemicals such as dioxins from PVC combustion has caused concern in other incineration scenarios, however, based on the available literature, it is considered that these compounds should be destroyed at the very high treatment temperatures relevant to this study (>1500 °C) [53–58]. Further detailed study, outside the scope of this work, will be necessary to fully quantify off-gas burdens.

5. Conclusions

This study demonstrated proof of concept for thermal treatment of PCM wastes, representative of those present on the Sellafield site, by vitrification with the addition of ground granulated blast-furnace slag, with a PCM waste to additive ratio of 3:1 by weight. The nature of the product wasteforms was influenced by the type of PCM waste and crucible containment. High metal feeds necessitated the use of clay/graphite crucibles, imposing a reducing environment, leading to a combined slag/metal wasteform; the slag component was thus strongly depleted in Fe_2O_3. Feeds with a lower fraction of metal could be processed in alumina crucibles, leading to a slag wasteform for the PVC and masonry wastes, and a combined slag/metal wasteform for the mixed waste type (with a higher metal fraction). Overall, the approach developed here would be compatible with commercially available batch wise in container and plasma vitrification technologies, described elsewhere [3,12,59]. Ce, as Pu surrogate was found to partition overwhelmingly (>97%) within the slag component, where a metal component was also present. Within the slag component, Ce was found to be incorporated primarily within the $CaO–Fe_2O_3–Al_2O_3–SiO_2$ glass phase with trace incorporation in other crystalline phases. The bulk speciation of Ce was determined to be Ce^{3+}, comparable with the known speciation of Pu^{3+} silicate glasses produced at high temperature. The upper analysed Ce_2O_3 concentration in the glass phase (1.2 mol% for the PVC waste) was well below the reported solubility limit of Ce_2O_3 and Pu_2O_3 in (boro)silicate glasses (ca. 2 mol%) processed at comparable temperature. Therefore, it is reasonable to expect that the slag component of the wasteforms developed here could incorporate Pu at the concentrations expected from treatment of PCM wastes. The estimated volume reduction factors of 80–95% demonstrated in this proof of concept investigation, utilising a 3:1 ratio of PCM waste to GGBS, by weight, produced slag wasteform volumes commensurate with the estimated maximum desirable volume reduction factor of 98%, based on criticality considerations (relative to untreated PCM waste, packaged in 200 L drums). The dissolution behaviour of the slag wasteforms in saturated $Ca(OH)_2$ (to simulate the hyperalkaline conditions of a cementitious GDF), proved similar to that of UK ILW waste glasses considered potentially suitable for geological disposal. Depletion of Ca from solution was inferred to be the consequence of reaction with the hydrated glass surface to form a calcium silicate hydrate (CSH) phase. The volume reduction and high durability of the PCM slags reported in this study, combined with the low solubility of actinides, under the hyperalkaline conditions of a UK ILW GDF, appear promising for application.

Acknowledgements

This research was primarily sponsored by Sellafield Ltd. and the Engineering and Physical Sciences Research Council through The University of Sheffield Knowledge Transfer Account, grant number EP/H500170/1. Use of the National Synchrotron Light Source, Brookhaven National Laboratory, was supported by the US Department of Energy, Office of Science, Office of Basic Energy Sciences, under Contract no. DE-AC02-98CH10886. NCH is grateful to The Royal Academy of Engineering and Nuclear Decommissioning Authority for funding. NCH gratefully acknowledge part support from the Engineering and Physical Sciences Research Council under grant numbers EP/I012214/1 and EP/G037140/1. CLC is grateful to The University of Sheffield for award of a Vice Chancellor's Fellowship.

References

[1] Department of Energy & Climate Change (DECC) and the Nuclear Decommissioning Authority (NDA), The 2010 UK Radioactive Waste Inventory: Main Report, NDA/DECC, Report NDA/ST?STY(11)0004, February 2011.
[2] M. Egan, A. Paulley, G. Towler, Treatment of Plutonium Contaminated Material at Sellafied: Best Practical Environmental Option Study, Sellafield Document Reference: RPLPSERP-000_PROJ_00165_V2, 2008. <http://www.sellafieldsites.com/wp-content/uploads/2012/08/PCM-BPEO-Study-QRS-1372A-1-Version-2_0.pdf>.
[3] N.C. Hyatt, S. Morgan, M.C. Stennett, C.R. Scales, D. Deegan, Mater. Res. Soc. Symp. Proc. 985 (2007) 393–398.
[4] P.A. Bingham, N.C. Hyatt, R.J. Hand, C.R. Wilding, Mater. Res. Soc. Symp. Proc. 1124 (2009) 161–166.
[5] P.A. Bingham, A.J. Connelly, R.J. Hand, N.C. Hyatt, Nucl. Future 6 (2010) 250–254.
[6] A.J. Connelly, R.J. Hand, P.A. Bingham, N.C. Hyatt, J. Nucl. Mater. 408 (2011) 188–193.
[7] P.A. Bingham, A.J. Connelly, R.J. Hand, N.C. Hyatt, Glass Technol. Part A 53 (2012) 83–100.
[8] P.A. Bingham, N.C. Hyatt, R.J. Hand, S.D. Forder, Glass Technol. Part A 54 (2013) 1–19.
[9] O.J. McGann, P.A. Bingham, R.J. Hand, A.S. Gandy, M. Kavčič, M. Žitnik, K. Bučar, R. Edge, N.C. Hyatt, J. Nucl. Mater. 429 (2012) 353–367.
[10] C.A. Utton, S.W. Swanton, J. Schofield, R.J. Hand, A. Clacher, N.C. Hyatt, Min. Mag. 76 (2012) 46–57.
[11] C.A. Utton, R.J. Hand, P.A. Bingham, N.C. Hyatt, S.W. Swanton, S.J. Williams, J. Nucl. Mater. 435 (2013) 112–122.
[12] N.C. Hyatt, M. James, Nucl. Eng. Int. (February 2013) 10–14.
[13] P.A. Bingham, R.J. Hand, M.C. Stennett, N.C. Hyatt, M.T. Harrison, Mater. Res. Soc. Symp. Proc. 1107 (2008) 421–428.
[14] C. Lopez, X. Deschanels, J.M. Bart, J.M. Boubals, C. Den Auwer, E. Simoni, J. Nucl. Mater. 312 (2003) 76–80.
[15] I.S. Muller, A.S. Buechele, F. Perez-Cardenas, H. Gan, I.L. Pegg, Mater. Research Soc. Symp. Proc. 556 (1999) 271–278.
[16] D.D. Keiser, D.P. Abraham, W. Sinkler, J.W. Richardson, S.M. McDeavitt, J. Nucl. Mater. 279 (2000) 234–244.
[17] D.P. Abraham, S.M. McDeavitt, J. Park, Annual meeting of the American Nuclear Society (ANS), Reno, NV (United States), 16–20 June 1996.
[18] T.B. Massalski, H. Okamoto, P. R. Subramanian, L. Kacprzak, Binary Alloy Phase Diagrams, second ed., ASM International, OH, USA, 1990.

[19] E.T. Turkdogan, Physicochemical Properties of Molten Slags and Glasses, The Metals Society, London, 1983.
[20] J. Chipman, Metall. Trans. 3 (1972) 55–64.
[21] G. Roberts, G. Krauss, R. Kennedy, Tool Steels, fifth ed., ASM International, OH, USA, 1998.
[22] C. Shi, J. Mater. Civil Eng. 16 (2004) 230–236.
[23] A.I. van Hoorn, J.T. van Konynenburg, P.J. Kreyger, Role of slag in basic oxygen steelmaking processes, in: W.K. Lu (Ed.), McMaster University Press, Hamilton, Ontario, 1976.
[24] D.E. Owen, J.E. Flinn, Idaho National Laboratory, Report RE-M-81-004, 1981.
[25] G.A. Reimann, J.D. Grandy, T.L. Eddy, G.L. Anderson, Idaho National Laboratory, Report EGG-WTD-10056, 1992.
[26] G.A. Reimann, P.C. Kong, Idaho National Laboratory, Report EGG-MS-10642, 1993.
[27] N. Marriott, S. Jones, M. Orhon, E. Akmoran, T. Gun, C. Cabuk, S. Materowski, Glass Technol. Part A 48 (2007) 290–296.
[28] Standard Test Methods for Determining Chemical Durability of Nuclear, Hazardous and Mixed Waste Glasses and Multiphase Glass Ceramics: the Product Consistency Test (PCT), Designation: C-1285-02, ASTM Int., West Conshohocken, PA, 2008.
[29] J.C. Woicik, B. Ravel, D.A. Fischer, W.J. Newburgh, J. Synchrotron Radiat. 17 (2010) 409–413.
[30] B. Ravel, M. Newville, ATHENA, ARTEMIS, J. Synchrotron Radiat. 12 (2005) 537–541.
[31] L.H. Van Vleck, Elements of Materials Science and Engineering, sixth ed., Addison Wesley Publishing, 1990.
[32] D.L. Parkhurst, C.A.J. Appelo, User's guide to PHREEQC (2003).
[33] R.J. Hand, R.J. Short, S. Morgan, N.C. Hyatt, G. Mobus, W.E. Lee, Glass Technol. 46 (2005) 121–124.
[34] R.J. Short, R.J. Hand, N.C. Hyatt, Mater. Res. Soc. Symp. Proc. 757 (2003) 141–146.
[35] R.J. Short, R.J. Hand, N.C. Hyatt, G. Mobus, J. Nucl. Mater. 340 (2005) 179–186.
[36] A. Bianconi, A. Marcelli, H. Dexpert, R. Karnatak, A. Kotani, T. Jo, J. Petiau, Phys. Rev. B 35 (1987) 806–812.
[37] A. Soldatov, T. Ivanchenko, S. Dellalonga, A. Kotani, Y. Iwamoto, A. Bianconi, Phys. Rev. B 50 (1994) 5074–5080.
[38] M.C. Stennett, C.L. Freeman, A.S. Gandy, N.C. Hyatt, J. Solid State Chem. 192 (2012) 172–178.
[39] D.P. Reid, M.C. Stennett, N.C. Hyatt, J. Solid State Chem. 191 (2012) 2–9.
[40] M.C. Stennett, C.L. Corkhill, L.A. Marshall, N.C. Hyatt, J. Nucl. Mater. 432 (2013) 182–188.
[41] X. Feng, H. Li, L.L. Li, J.G. Darab, M.J. Schweiger, J.D. Vienna, B.C. Buncker, P.G. Allen, J.J. Bucher, I.M. Craig, N.M. Edelstein, D.K. Shuh, R.C. Ewing, L.M. Wang, E.R. Vance, Ceram. Trans. 93 (1999) 409–419.
[42] N.E. Bibler, W.G. Ramsey, T.F. Meaker, J.M. Pareizs, Mater. Res. Soc. Symp. Proc. 412 (1996) 65–74.
[43] J.K. Bates, A.G. Ellison, J.W. Emery, J.C. Hoh, Mater. Res. Soc. Symp. Proc. 412 (1996) 57–64.
[44] T. Chave, P. Frugier, S. Gin, A. Ayral, Geochim. Cosmochim. Ac. 75 (2011) 4125–4139.
[45] Why a cementitious repository?, United Kingdom Nirex Limited, Report N/034, June 2001.
[46] T.M. El-Shamy, Phys. Chem. Glasses 14 (1973) 1–5.
[47] D. Rai, M. Yui, A. Kitamura, B. Grambow, J. Solution Chem. 40 (2011) 1473–1504.
[48] F.T. Ewart, J.L. Smith-Briggs, H.P. Thomason, S.J. Williams, Waste Manage. 12 (1992) 241–252.
[49] J.A. Berry, J. Hobley, S.A. Lane, A.K. Littleboy, M.J. Nash, P. Oliver, J.L. Smith-Briggs, S.J. Williams, Analyst 114 (1989) 339–347.
[50] B. Kursten, E. Smailos, I. Azkarate, L. Werme, N.R. Smart, G. Marx, M.A. Cunado, G. Santarini, Corrosion evaluation of metallic materials for long-lived HLW/spent fuel disposal containers: review of 15–20 years of research, EU project report, 2002.
[51] C. Altenhein-Haese, H. Bischoff, L. Fu, J. Mao, G. Marx, J. Alloys Compd. 213–214 (1994) 554–556.
[52] A. Pearson, Personal Commun. 17 (6) (2013).
[53] I.C. McNeill, L. Memetea, W.J. Cole, Polym. Degrad. Stabil. 49 (1995) 181–191.
[54] E. Gomez, D.A. Rani, C.R. Cheeseman, D. Deegan, M. Wise, A.R. Boccaccini, J. Hazard Mater. 161 (2009) 614–626.
[55] Green Paper on Environmental issues of PVC, European Commission Environment, COM (2000) 469, Brussels, 26.7.2000.
[56] S.M. Al-Salem, P. Lettieri, J. Baeyens, Prog. Energy Combust. 36 (2010) 103–129.
[57] J.K. Fink, J. Anal. Appl. Pyrol. 51 (1999) 239–252.
[58] M. Asanuma, M. Kajioka, M. Kuwabara, Y. Fukumoto, K. Terada, Establishment of Advanced Recycling Technology, JFE Technical Report, No. 13, 2009. <http://www.jfe-steel.co.jp/en/research/report/013/pdf/013-07.pdf>.
[59] K. Witwer, S. Woosley, B. Campbell, M. Wong, J. Hill, GeoMelt ICV Treatment of Sellafield Pond Solids Waste, in: Proceedings of Waste Management 2013 Conference, Phoenix, AZ, February 24–28, 2013.